

# Forecasting with time series imaging

Xixi Li<sup>a,1</sup>, Yanfei Kang<sup>a,1</sup>, Feng Li<sup>b,\*</sup>

<sup>a</sup>*School of Economics and Management, Beihang University, Beijing 100191, China.*

<sup>b</sup>*School of Statistics and Mathematics, Central University of Finance and Economics, Beijing 102206, China.*

---

## Abstract

Feature-based time series representations have attracted substantial attention in a wide range of time series analysis methods. Recently, the use of time series features for forecast model averaging has been an emerging research focus in the forecasting community. Nonetheless, most of the existing approaches depend on the manual choice of an appropriate set of features. Exploiting machine learning methods to extract features from time series automatically becomes crucial in state-of-the-art time series analysis. In this paper, we introduce an automated approach to extract time series features based on time series imaging. We first transform time series into recurrence plots, from which local features can be extracted using computer vision algorithms. The extracted features are used for forecast model averaging. Our experiments show that forecasting based on automatically extracted features, with less human intervention and a more comprehensive view of the raw time series data, yields highly comparable performances with the best methods in the largest forecasting competition dataset (M4) and outperforms the top methods in the Tourism forecasting competition dataset.

*Keywords:* Forecasting, Time series imaging, Time series feature extraction, Recurrence plots, Forecast combination.

---

## 1. Introduction

Time series *features* are a collection of statistical representations of time series characteristics. Feature-based time series representation has attracted remarkable attention in a vast majority of data mining tasks for time series. Most of the time series problems, including time series clustering (e.g., Wang et al., 2006; Bandara et al., 2020), classification (e.g., Fulcher and Jones, 2014; Nanopoulos et al., 2001) and anomaly detection (e.g., Hyndman et al., 2015; Talagala, Hyndman, Smith-Miles, Kandanaarachchi and Muñoz, 2019; Corizzo et al., 2020),

---

\*Corresponding author

*Email addresses:* [lixixi199407@buaa.edu.cn](mailto:lixixi199407@buaa.edu.cn) (Xixi Li), [yanfeikang@buaa.edu.cn](mailto:yanfeikang@buaa.edu.cn) (Yanfei Kang), [feng.li@cufe.edu.cn](mailto:feng.li@cufe.edu.cn) (Feng Li)

*URL:* <https://orcid.org/0000-0001-5846-3460> (Xixi Li), <https://orcid.org/0000-0001-8769-6650> (Yanfei Kang), <https://orcid.org/0000-0002-4248-9778> (Feng Li)

<sup>1</sup>The authors contributed equally.

are eventually attributed to the quantification of similarity among time series data using time series feature representations. [Fulcher \(2018\)](#) presents thousands of interpretable features that can be used to represent a time series, such as global features, subsequence features and other hybrid features, for classifying time series ([Fulcher and Jones, 2014](#)) and labeling the emotional content of speech ([Fulcher et al., 2013](#)). [Christ et al. \(2018\)](#) compute 794 time series features based on hypothesis tests and illustrate their applications in time series anomaly detection and classification. Another line of approaches for time series feature extraction is by auto-encoder models (e.g., [Vincent et al., 2008](#)). [Corizzo et al. \(2020\)](#) further exploit time series features extracted from auto-encoder models for gravitational waves detection. Other recent studies use auto-encoder models for feature representation in time series forecasting (e.g., [Laptev et al., 2017](#); [Abdollahi et al., 2020](#)).

Instead of the traditional time series forecasting procedure – fitting a model to the historical data and simulating future data based on the fitted model, selecting the most appropriate forecasting model or averaging a number of candidate models based on time series features has been a popular alternative approach. In the last few decades, many attempts have been made on the feature-based model selection and averaging procedures for univariate time series forecasting. For example, [Collopy and Armstrong \(1992\)](#) provided 99 rules using 18 features to combine four extrapolation methods by examining a rule base to forecast annual economic and demographic time series; [Arinze \(1994\)](#) described the use of artificial intelligence techniques to improve the forecasting accuracy, built an induction tree to model time series features and developed the most accurate forecasting method; [Shah \(1997\)](#) constructed several individual selection rules for forecasting using discriminant analysis based on 26 time series features; [Meade \(2000\)](#) used 25 summary statistics of time series as explanatory variables in predicting the relative performances of nine forecasting methods based on a set of simulated time series with known properties; [Petropoulos et al. \(2014\)](#) proposed “horses for courses” and measured the effects of seven time series features on the forecasting performances of 14 popular forecasting methods on the monthly data in the M3 dataset ([Makridakis and Hibon, 2000](#)); more recently, [Kang et al. \(2017\)](#) visualized the performances of different forecasting methods in a two-dimensional principal component feature space and provided a preliminary understanding of their relative performances. [Talagala et al. \(2018\)](#) presented a general framework for forecast model selection using meta-learning in which they utilize a random forest algorithm to select the best forecasting method based on time series features. [Montero-Manso et al. \(2020\)](#) trained a meta-model to obtain the weights of various forecasting methods and made a weighted forecasting combination. The input of the meta-model is a set of features calculated on the training data, while the output

is a group of weights assigned to each candidate forecasting method. Their method ranked 2nd in the M4 competition (Makridakis et al., 2020).

Having revisited the literature on feature-based time series forecasting, we find that (i) although researchers often highlight the usefulness of time series features in selecting the best forecasting method, most of the existing approaches depend on the manual choice of an appropriate set of features, which makes the forecast process that relies on the data and the expertise of the forecasters inflexible (Fulcher, 2018), and more importantly (ii) the current literature on feature-based forecasting focuses on global features of time series, leaving local characteristics under-emphasized. In some instances, the local dynamics of time series contain important information such as heart failure in medical signals and irregular weather changes. Therefore, exploiting automated feature extraction from time series data becomes vital. Inspired by the recent work of Hatami et al. (2017) and Wang and Oates (2015) in time series classification tasks, this paper aims to explore time series forecasting based on model averaging with the idea of time series imaging, from which time series global and local features can be automatically extracted using computer vision algorithms. The proposed approach also enables automated feature extraction. This novel approach for time series forecasting is more flexible than forecasting based on manually curated time series features.

The rest of the paper is organized as follows. Section 2 presents our feature extraction method for time series imaging. In Section 3, we describe how to assign weights to a group of candidate forecasting methods using imaging-based time series features and perform forecast combination accordingly. Section 4 applies our imaging-based time series forecast combination method to two large collections of real datasets, namely the M4 competition dataset and the Tourism competition dataset. Section 5 provides our discussions and insights, as well as several possible future research directions. Section 6 concludes the paper.

## 2. Time series imaging and feature extraction

In this paper, we extract time series features based on time series imaging in two steps. In the first step, we encode the time series into images using recurrence plots. In the second step, time series features are extracted from images using image processing techniques. We consider two different image feature extraction approaches: spatial bag-of-features (SBoF) model and convolutional neural networks (CNNs). We describe the details in the following sections.

### 2.1. Time series imaging

We use recurrence plots (RPs) to encode time series data into images, which provides a way to visualize the periodic nature of a trajectory through a phase space (Eckmann et al., 1987)

and can contain all relevant dynamical information in the time series (Thiel et al., 2004). A recurrence plot of time series  $x$ , showing when the time series revisits a previous state, can be formulated as

$$R(i, j) = \Theta(\epsilon - \|x_i - x_j\|),$$

where  $R(i, j)$  is the element of the recurrence matrix  $R$ ,  $i$  indexes time on the x-axis of the recurrence plot, and  $j$  indexes time on the y-axis.  $\epsilon$  is a predefined threshold, and  $\Theta(\cdot)$  is the Heaviside step function. In short, one draws a black dot when  $x_i$  and  $x_j$  are closer than  $\epsilon$ . Instead of binary output, an un-thresholded RP is not binary but difficult to quantify. We use the following modified RP, which balances the binary output and un-thresholded RP.

$$R(i, j) = \begin{cases} \epsilon & \|x_i - x_j\| > \epsilon, \\ \|x_i - x_j\| & \text{otherwise.} \end{cases}$$

It gives more values than a binary RP and results in colored plots. Fig. 1 shows three typical examples of recurrence plots. They reveal different patterns of recurrence plots for time series with randomness, periodicity, chaos, and trend. We can see that the recurrence plots shown in the right column well depict the pre-defined patterns in the time series shown in the left column.

## 2.2. Feature extraction with the SBoF model

We propose an image-based time series feature extraction framework using the SBoF (spatial bag-of-features) model. As shown in Fig. 2, the framework consists of three steps: (i) detect key points with the scale-invariant feature transform (SIFT) algorithm (Lowe, 1999) and find basic descriptors with  $k$ -means; (ii) generate the representation based on the locality constrained linear coding (LLC) method (Wang et al., 2010); and (iii) extract spatial information via spatial pyramid matching (SPM) and pooling. We interpret the details in each step, respectively.

The original bag-of-features (BoF) model, which extracts features from one-dimensional signal segments, has achieved great success in time series classification (Baydogan et al., 2013; Wang et al., 2013). Hatami et al. (2017) transformed a time series into two-dimensional recurrence images with a recurrence plot (Eckmann et al., 1987) and then applied the BoF model. Extracting time series features is then equivalent to identifying key points in images, which are called key descriptors. A promising algorithm is the SIFT algorithm (Lowe, 1999), which is used to detect and describe local features in images by identifying the maxima/minima of the difference of Gaussians (DoG) that occur at the multiscale spaces of an image as its key descriptors. It consists of the following four steps.

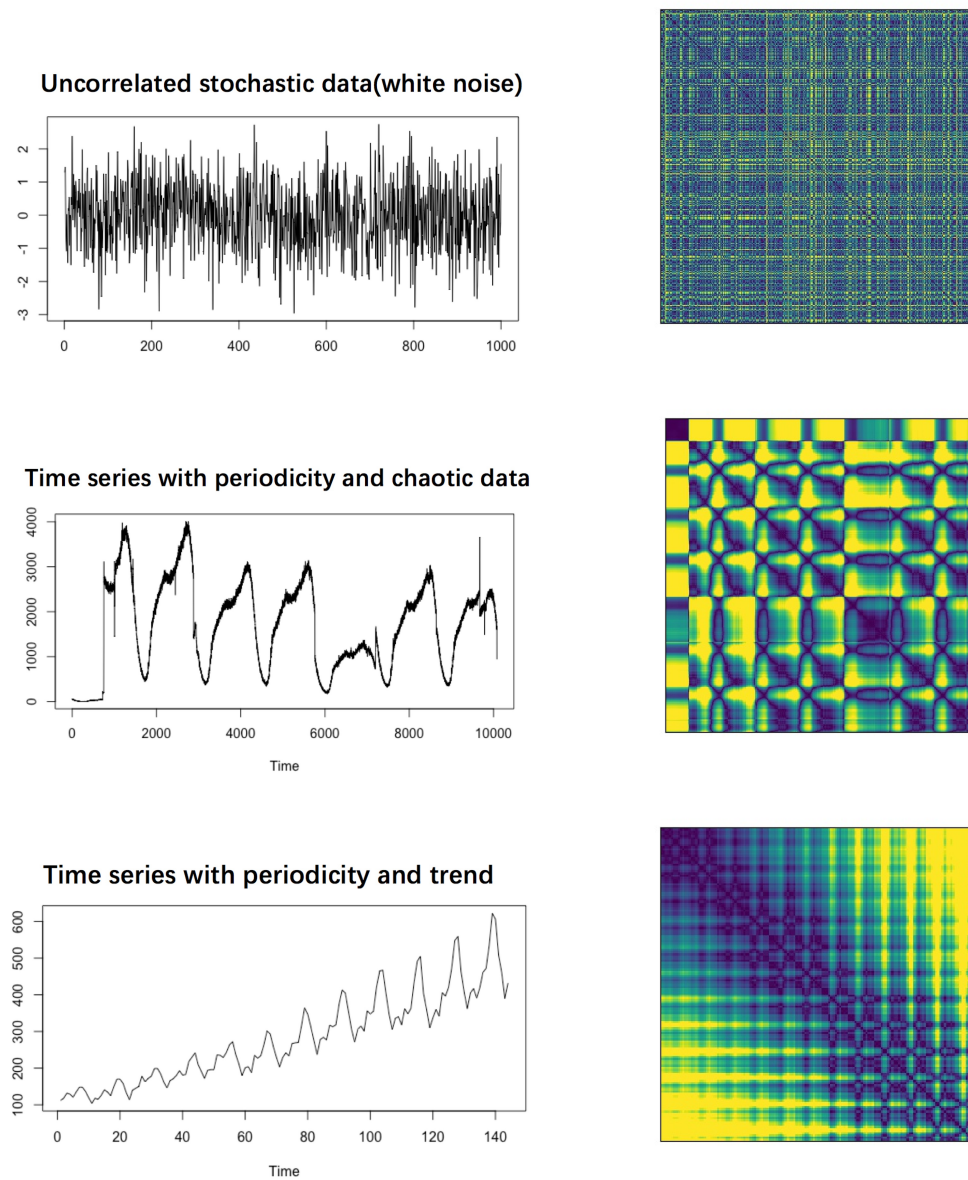


Figure 1. Typical examples of recurrence plots (right column) for time series data with different patterns (left column): uncorrelated stochastic data, i.e., white noise (top), a time series with periodicity and chaos (middle), and a time series with periodicity and trend (bottom).

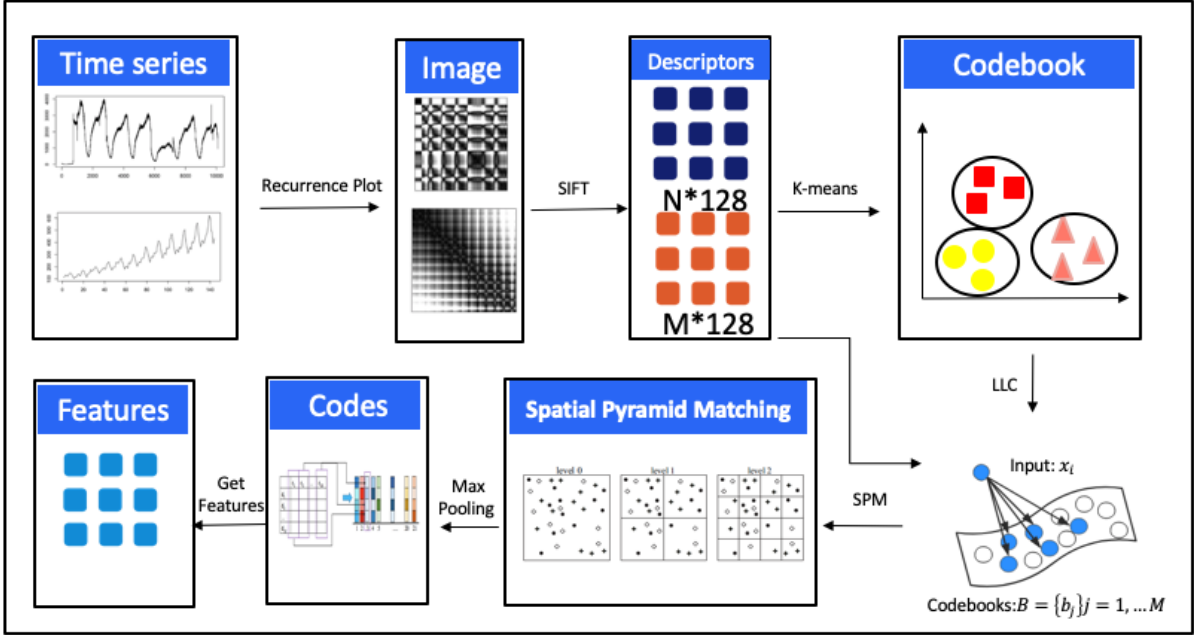


Figure 2. Image-based time series feature extraction with spatial bag-of-features model. It consists of four steps: (i) encode a time series as an image with recurrence plots; (ii) detect key points with SIFT and obtain the basic descriptors with  $k$ -means for the codebook; (iii) generate the representation based on LLC; and (iv) extract spatial information via SPM and max pooling.

1. **Detect extreme values in the scale spaces.** We search over all the scale spaces and use the Gaussian differential method to identify the potential interest points and select those invariant to scale and orientation.
2. **Find the key points.** The position scale is determined by fitting a model at each candidate position, and the key points are selected according to their stability.
3. **Assign feature directions.** This step assigns the key points one or more directions based on the local gradient direction of the image. All subsequent operations are about how to transform the direction, scale, and position of the key points to allow for invariance in the features.
4. **Describe key points.** Within the neighborhood around each feature point, the local gradient of the image is measured at selected scales, which is transformed into a representation that allows larger local shape deformations and illumination transformations. The SIFT method uses a 128-dimensional vector to characterize the key descriptors in an image. First, an 8-direction histogram is established in each  $4 \times 4$  subregion, and 16 subregions around the key points are used. We then calculate the magnitude and direction of each pixel's gradient magnitude and add it to the corresponding subregion. In the end, 128-dimensional image data based on histograms are generated.

Each descriptor can be projected onto its local coordinate system, and the projected coordinates are integrated by max pooling to generate the final representation with the LLC method, which utilizes the locality constraints to project each descriptor onto its local coordinate system (Wang et al., 2010). The projected coordinates are integrated by max pooling to generate the final representation:

$$\min_c \sum_i^N \|x_i - Bc_i\|^2 + \lambda \|d_i \odot c_i\|^2, \text{ s.t. } 1^T c_i = 1, \forall i, \quad (1)$$

where  $d_i = \exp(\text{dist}(x_i, B)/\sigma)$  and  $x_i \in R^{128 \times 1}$  is the vector of one descriptor. The basic descriptors  $B \in R^{128 \times M}$  are obtained by  $k$ -means clustering. The representation parameters  $c_i$  are used as time series representations through Equation (1). The locality adaptor  $d_i$  gives different freedom for each basis vector proportional to its similarity to the input descriptor. We use  $\sigma$  to adjust the weight decay speed for the locality adaptor, and  $\lambda$  is the adjustment factor. However, in reality, the number of descriptors obtained by the SIFT algorithm is usually huge. To address this problem, Wang et al. (2010) proposed an incremental codebook optimization method for LLC.

The bag-of-features model calculates the distribution characteristics of feature points in the whole image and then generates a global histogram. As a result, the image’s spatial distribution information is lost, and the image may not be accurately described. To obtain the spatial information of images, we apply a spatial pyramid matching (SPM) method, which statistically distributes image feature points at different resolutions and has achieved high accuracy on a large dataset of 15 natural scene categories (Lazebnik et al., 2006). The image is divided into progressively finer grid sequences at each level of the pyramid, and features are derived from each grid and combined into one large feature vector. Fig. 3 depicts the diagram of the SPM and max pooling process. In this task, we divide the image by  $1 \times 1$ ,  $2 \times 2$  and  $4 \times 4$ , and thus obtain 21 subregions. To obtain the representation for each subregion, we first obtain the descriptors. Suppose that we obtain 12 descriptors denoted by  $D_i \in R^{12 \times 200}$  for the third region (the dimension of the local linear representation of the descriptors is equal to 200). We then can obtain the maximum value of every dimension of  $D_i$ . After max pooling, we calculate the feature representation denoted by  $f_i \in R^{200 \times 1}$  for the third region. The feature representations of the other twenty regions can be obtained in the same way. Finally, the 21 features are linked together for the final representation of the time series. In this way, the final size of the feature vectors is  $21 \times 200 = 4200$ . More details about the experimental setup in the SoBF model can be found in Appendix A.



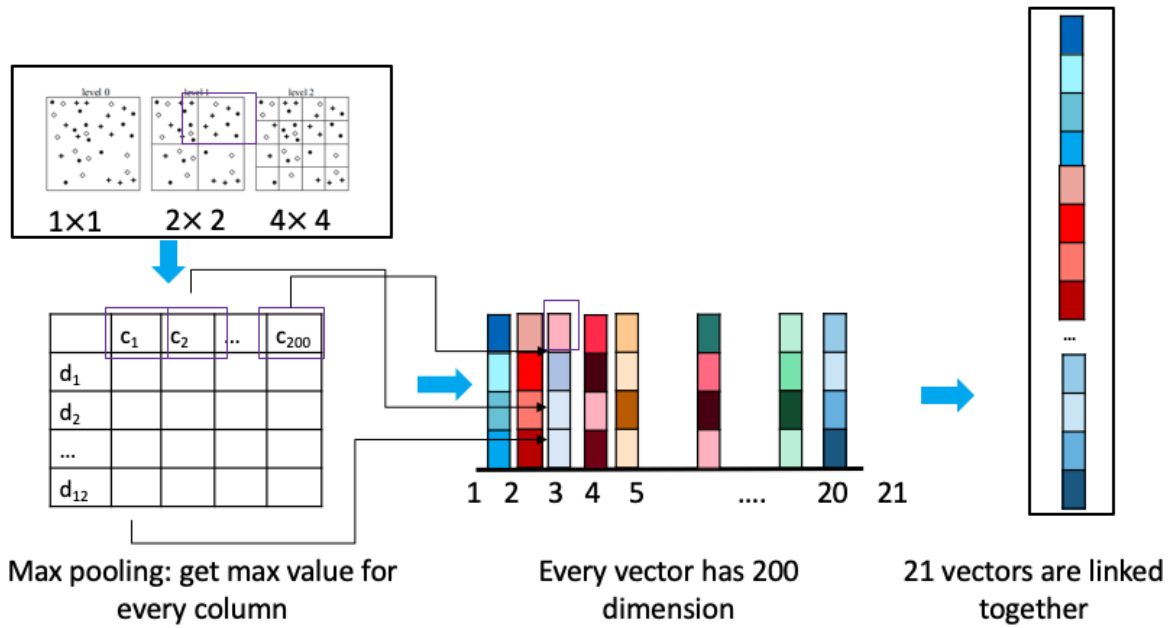


Figure 3. Spatial pyramid matching and max pooling. The image is divided into progressively finer grid sequences at each level of the pyramid, and features are derived from each grid and combined into one large feature vector. We divide the image by  $1 \times 1$ ,  $2 \times 2$  and  $4 \times 4$ , and thus obtain 21 subregions. We first obtain the descriptors for each region. Suppose that we obtain 12 descriptors denoted by  $D_i \in R^{12 \times 200}$  for the third region (200 is the dimension of the local linear representation of the descriptor). Then, we can obtain the maximum value of every dimension of  $D_i$ . After max pooling, we obtain the feature representation denoted by  $f_i \in R^{200 \times 1}$  for the third region. The feature representations of the other 20 regions can be obtained in the same way. Finally, the 21 features are linked together for the final representation for the time series.



### 2.3. Feature extraction with fine-tuned deep neural networks

An alternative to SBoF for image feature extraction is to use a deep CNN, which has achieved great breakthroughs in image processing (Krizhevsky et al., 2012). For example, Berkeley researchers (Donahue et al., 2014) proposed feature extraction methods called DeCAF (a deep convolutional activation feature for generic visual recognition) and directly used deep convolutional neural networks for feature extraction. Their experimental results show that the extracted features yield higher accuracy than traditional image features. In addition, some researchers (e.g., Razavian et al., 2014) use the features acquired by convolutional neural networks as the input of an image classifier, which significantly improves the image classification accuracy.

Nonetheless, the performance of neural networks heavily depends on the setting of the network structure and the hyper-parameters. A deeper layer is often essential for achieving higher performance in a task. As a result, extensive computational power is needed. An appealing feature of our time series imaging approach is that a large number of well pre-trained neural network models for imaging classification exist. We could easily transfer the model to our task via transfer learning (Pan and Qiang, 2010), which has been widely used recently in a variety of fields such as image classification (Han et al., 2018) and natural language processing (Ahmad et al., 2020). To simplify our task, we use the fine-tuning approach (Ge and Yu, 2017) from the field of transfer learning. In short, it uses pre-trained networks and makes adjustments to our tasks. We fix the parameters of the previous layers based on the pre-trained model with ImageNet data and fine-tune the last few layers for our task. In general, the closer the layer is to the first layer, the more general features can be extracted; the closer the layer is to the back layer, the more specific features for classification tasks can be extracted. In this way, the computational efficiency of network training can be significantly accelerated.

Fig. 4 shows the framework of transfer learning with fine-tuning. In this task, the deep network is trained on the large ImageNet dataset (Deng et al., 2009), and the pre-trained network is publicly available. Specifically, we fix the weights of all the previous layers of the pre-trained network except for the last fully connected layers and then use our time series images as inputs. Finally, the high-dimensional features of the time series images can be obtained from the pre-trained network. We consider the following representative architectures in our experiments: *ResNet-v1-101* (He et al., 2016), *ResNet-v1-50* (He et al., 2016), *Inception-v1* (Szegedy et al., 2015), and *VGG-19* (Simonyan and Zisserman, 2014). The dimensions of the time series features obtained from the pre-trained *ResNet-v1-101*, *ResNet-v1-50*, *Inception-v1* and *VGG-19* architectures are 2048, 2048, 1024 and 1000, respectively. More details about the experimental setup in the CNN-based feature extraction can be found in Appendix A.

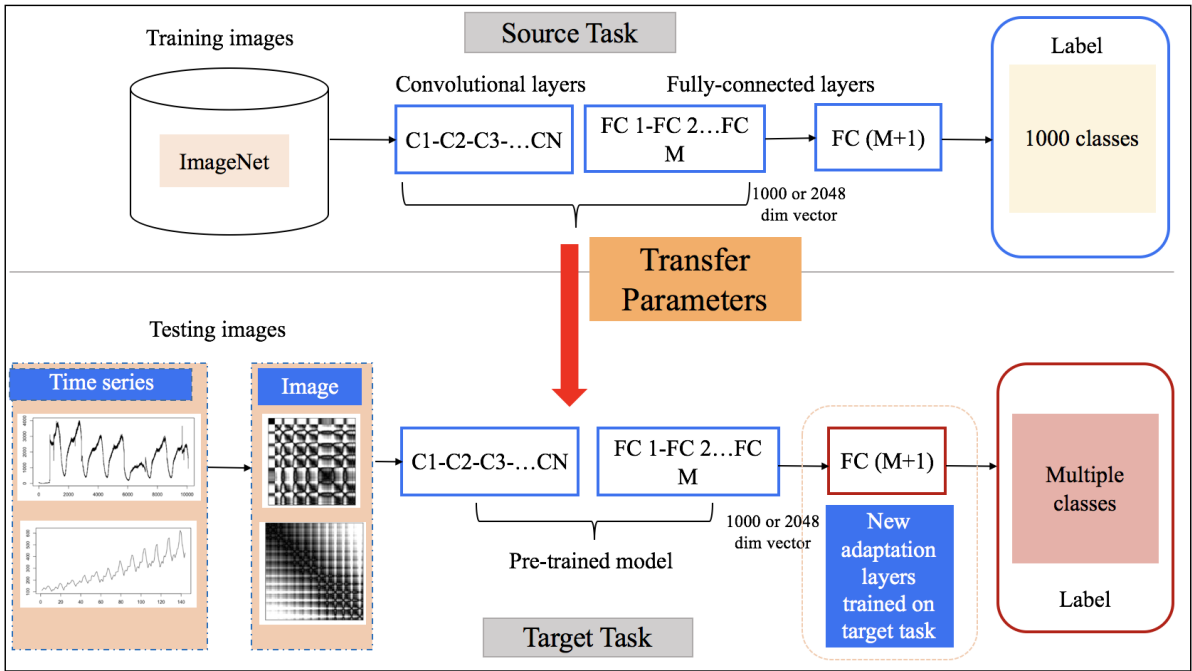


Figure 4. Framework of transfer learning with fine-tuning. Classic CNN models are trained on a large dataset (ImageNet). For the CNN model, the closer the layer is to the first layer, the more general features can be extracted; the closer the layer is to the back layer, the more specific features for classification tasks can be extracted. To extract time series features, we fix the parameters of all the previous layers except for the last fully connected layer, and fine-tune the last layer for our task. With the trained model, we obtain the final representation of the time series.

### 3. Time series forecasting with image features

We aim to find the optimal combination of a pool of candidate forecasting methods. The essence is to link the knowledge of forecasting errors from different forecasting methods to time series features. Therefore, in this section, we focus on the mapping from the time series image features to forecasting method performances. We use nine most popular time series forecasting methods as candidates for forecast combination, which are also used in many recent studies (Montero-Manso et al., 2020; Talagala, Li and Kang, 2019; Kang et al., 2020). They are the automated ARIMA algorithm (ARIMA), automated exponential smoothing algorithm (ETS), feed-forward neural network using autoregressive inputs (NNET-AR), exponential smoothing state space model with a Box-Cox transformation (TBATS), seasonal and trend decomposition using LOESS with AR modeling of the seasonally adjusted series (STLM-AR), random walk with drift (RW-DRIFT), theta method (THETA), naïve (NAIVE), and seasonal naïve (SNAIVE). They are described in Table 1 and implemented in the **R** package `forecast` (Hyndman et al., 2019).

To validate the effectiveness of our image features of the time series, we follow the work of Montero-Manso et al. (2020), who proposed a model-averaging method based on 42 manually curated time series features and won the second place in the M4 competition (Makridakis et al., 2020), to obtain the weights for forecast combination based on our image features. To make our proposed method comparable with those in M4, we use the overall weighted average (OWA) to measure the forecasting accuracies, as used in the M4 competition. OWA is an overall indicator of two accuracy measures, the mean absolute scaled error (MASE) and the symmetric mean absolute percentage error (sMAPE). The individual measures are calculated as follows.

$$\begin{aligned}
 \text{sMAPE} &= \frac{1}{h} \sum_{t=1}^h \frac{2 | Y_t - \hat{Y}_t |}{| Y_t | + | \hat{Y}_t |}, \\
 \text{MASE} &= \frac{1}{h} \frac{\sum_{t=1}^h | Y_t - \hat{Y}_t |}{\frac{1}{n-m} \sum_{t=m+1}^n | Y_t - Y_{t-m} |}, \\
 \text{OWA} &= \frac{1}{2} (\text{sMAPE}/\text{sMAPE}_{\text{Naive2}} + \text{MASE}/\text{MASE}_{\text{Naive2}}),
 \end{aligned} \tag{2}$$

where  $Y_t$  is the real value of the time series at point  $t$ ,  $\hat{Y}_t$  is the point forecast,  $h$  is the forecasting horizon, and  $m$  is the frequency of the data (e.g., 4 for quarterly series). Naïve2 is equivalent to the Naïve (NAIVE) method but applied to the time series adjusted for seasonal factors.

Our framework for model averaging is shown in Fig. 6. It consists of two parts. In the training process, based on the extracted image features and the OWA values of the nine forecasting methods, we train a feature-based gradient tree boosting model (XGBoost, Chen and Guestrin, 2016), to produce nine weights for forecast model averaging by minimizing the OWA

Table 1. The methods used for forecast combination. All these methods are implemented using the `forecast` package in the **R** software.

Forecasting method	Description	<b>R</b> implementation
ARIMA	The autoregressive integrated moving average model automatically estimated in the <code>forecast</code> package for <b>R</b> (Hyndman and Khandakar, 2008).	<code>auto.arima()</code>
ETS	The exponential smoothing state space model (Hyndman et al., 2002).	<code>ets()</code>
NNET-AR	A feed-forward neural network using autoregressive inputs.	<code>nnetar()</code>
TBATS	The exponential smoothing state space model with a Box-Cox transformation, ARMA errors, trend and seasonal components (De Livera et al., 2011).	<code>tbats()</code>
STLM-AR	The STL decomposition (Cleveland et al., 1990) with AR modeling of the seasonally adjusted series.	<code>stlm(..., model = ar)</code>
RW-DRIFT	The random walk model with drift.	<code>rwf(..., drift = TRUE)</code>
THETA	The decomposition forecasting model by modifying the local curvature of the time-series through a coefficient ‘Theta’ that is applied directly to the second differences of the data (Assimakopoulos and Nikolopoulos, 2000).	<code>thetaf()</code>
NAIVE	The naïve method, which takes the last observation as the forecasts of all the forecast horizons.	<code>naive()</code>
SNAIVE	The seasonal naïve method, which forecasts using the most recent values of the same season.	<code>snaive()</code>

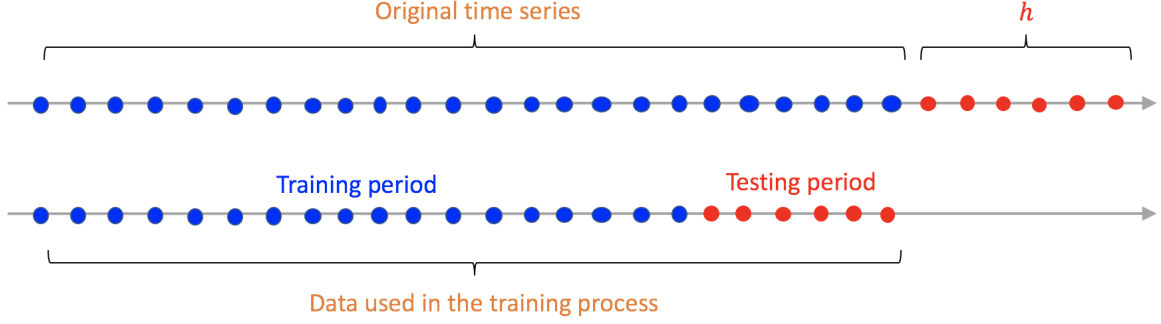


Figure 5. The temporal holdout strategy used to generate the training dataset. Each original time series is divided into a training period and a testing period. The length of the testing period is equal to the forecasting horizon ( $h$ ) given by the M4 competition. We calculate time series image features from the training periods of the training dataset, generate forecasts, and compute the corresponding OWA values over the test periods for each candidate forecasting method. We train an XGBoost model on the training dataset and obtain weights for each candidate forecasting method, which are then used to generate forecasts by forecast combination for the future data.

error obtained by forecast combination. Let  $f_n$  be the image features extracted from a time series, and  $N$  is the total number of the time series.  $O_{nm}$  is the contribution to the OWA error of  $m$ -th method for the series  $n$ -th time series.  $p(f_n)_m$  is the output of the XGBoost algorithm corresponding to  $m$ -th forecasting method, based on the features extracted from the  $n$ -th time series. The gradient tree boosting approach minimizes the weighted average loss function as

$$\arg \min_w \sum_{n=1}^N \sum_{m=1}^M w(f_n)_m O_{nm},$$

where  $w(f_n)_m$  are the softmax-transformed weights for the output  $p(f_n)_m$  of the XGBoost model defined as

$$w(f_n)_m = \frac{\exp\{p(f_n)_m\}}{\sum_m \exp\{p(f_n)_m\}}.$$

The hyper-parameter settings for XGBoost are available in Appendix B.

In the testing process, we use the trained model and the image features extracted from the testing data to obtain the weights of different forecasting models. Finally, based on the weights and forecasts of different models, we can obtain the final forecasts for the testing data.

## 4. Experiments

### 4.1. Forecasting with M4 competition data

The first dataset we use to evaluate our proposed method is a collection of general-purpose data from the M4 competition that consists of 100,000 time series diversely from the economic,

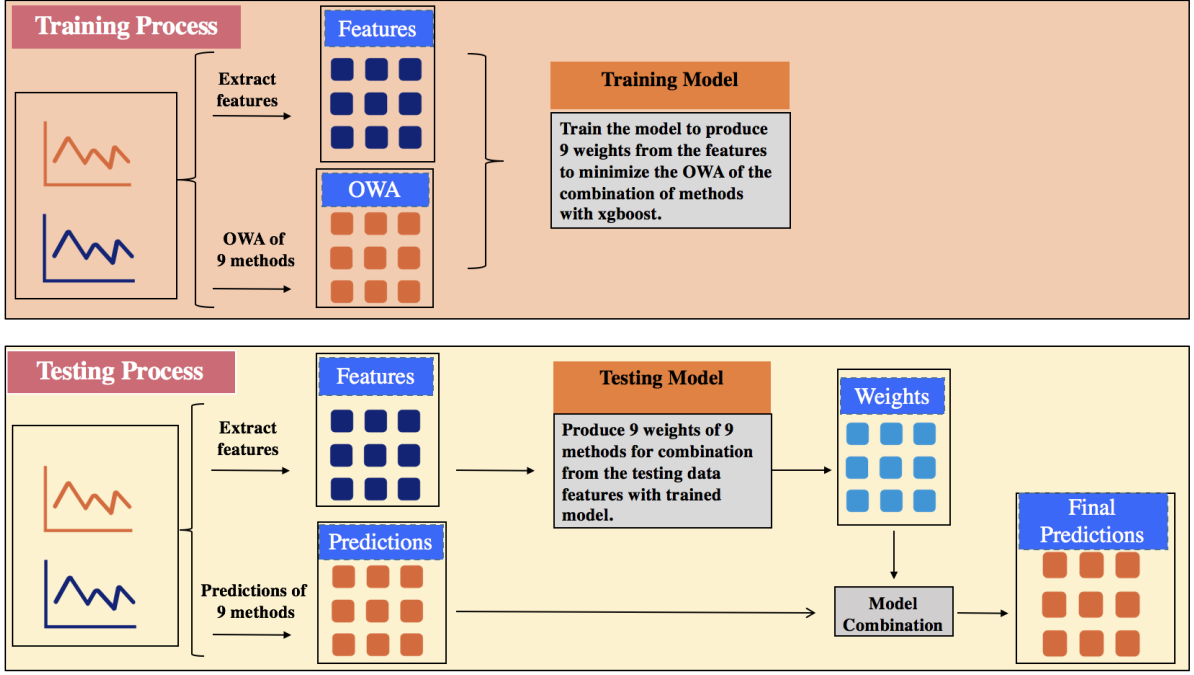


Figure 6. Framework of forecast model averaging based on automatic feature extraction. In the training process, nine weights are obtained for the forecast model combination using XGBoost. Based on the weights, we obtain the forecasts for the testing data in the testing process.

finance, demographics, and industry domains. In the training process, we divide the original time series in M4 into training and testing periods following the strategy in Fig. 5. The lengths of the testing periods are equal to the forecasting horizon ( $h$ ), i.e., 6 for yearly, 8 for quarterly, 18 for monthly, 13 for weekly 14 for daily, and 48 for hourly data, which are given by the M4 competition. For each time series in M4, we calculate time series features from the training period, generate forecasts, and compute the corresponding OWA values over the test period for each candidate forecasting method. We then train an XGBoost model to produce the weights for each forecasting method described in Table 1. In the testing process, we use the trained model to forecast the original M4 time series, and evaluate the forecasts based on the future M4 data, which are public after the M4 competition.

We now apply our imaging-based time series forecasting method to the M4 data. To illustrate that the extracted image features are diverse and can be used to characterize the original time series, we project the features of the time series with different periods into two-dimensional feature space using t-distributed stochastic neighbor embedding (t-SNE, Maaten (2014)). From Fig. 7, we notice that yearly, quarterly, monthly, daily and hourly data can be well distinguished in the feature spaces, although the features are automatically extracted from time series images.

Following the framework in Fig. 6, we obtain the forecasts of M4 based on time series imaging. Our model averaging results are compared with the results of the top ten ranked

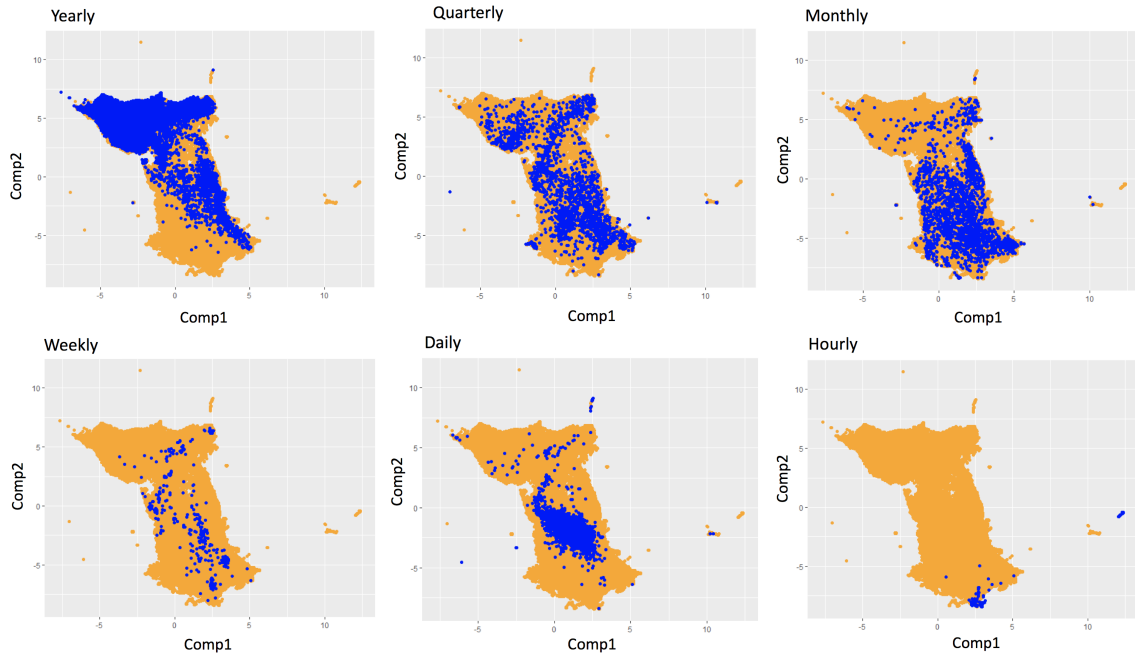


Figure 7. Two-dimensional feature spaces of the M4 time series with different periods. The blue points highlight areas where the time series instance (orange points) with the corresponding seasonal pattern lie.

Table 2. Description of the top ten forecasting methods in M4 competition (Makridakis et al., 2020).

Ranking	Description
1	A hybrid model mixing Exponential Smoothing (ES) with a black-box Recurrent Neural Network (RNN) forecasting engine (Smyl, 2020).
2	Weighted forecast combination of nine standard forecasting methods in Table 1 (Montero-Manso et al., 2020).
3	Weighted average of multiple statistical methods using hold-out tests (Pawlikowski and Chorowska, 2020).
4	Combination of multiple statistical methods as described in Armstrong (2001).
5	Weighted average of the standard ARIMA, ETS and THETA methods described in Table 1 (Fiorucci and Louzada, 2020).
6	Median of ETS, CES (Complex exponential smoothing, Svetunkov and Kourentzes, 2018), ARIMA, and THETA methods (Petropoulos and Svetunkov, 2020).
7	Combination of two THIEF (Temporal Hierarchical Forecasting, Athanasopoulos et al., 2017) forecasts (with the base model of ARIMA and THETA, respectively) (Shaub, 2020).
8	THETA method with data deseasonalization and Box-Cox Transformation.
9	A calibrated average of Rho and Delta (Card) forecasting methods (Doornik et al., 2020).
10	Forecast combination of seven benchmarks.



methods (Table 2) from the M4 competition, which are available in the concluding paper of M4 (Makridakis et al., 2020). Detailed descriptions and the code for replicating the top ten methods are available in the M4 GitHub repository (<https://github.com/Mcompetitions/M4-methods>). Note that the replication results may slightly differ due to the updates of related **R** packages. However, since the concluding paper of M4 competition (Makridakis et al., 2020) is publicly available at the same time of this work, the possible code changes in the **R** packages used by the competitors are negligible. Tables 3, 4 and 5 depict the MASE, sMAPE, and OWA values for our time series imaging method with model-averaging, and the top ten methods from the M4 competition. The optimal parameters of XGBoost on the M4 competition dataset can be found in Table 7 of Appendix B.

Overall, our model averaging method with automated time series image features can achieve highly comparable performances with the top methods from the M4 competition. From Table 5, our method ranks the sixth overall. But our approach has the advantages: (1) limited human interaction is required during feature extraction, (2) both global and local features are utilized, (3) the fine-tuned results from existing CNN models in the computer vision tasks can be seamlessly transferred to our model, and (4) it sheds the potential improvements of forecasting performance with the advances of neural networks for the computer vision tasks.

#### 4.2. Forecasting with the Tourism competition data

To validate our method’s generality and robustness in even specific forecasting domains, we now apply the proposed method to the Tourism competition dataset that consists of 366 monthly series, 427 quarterly series, and 518 yearly series (Athanasopoulos et al., 2011). In the training process, we use the M4 competition data as training data to train the XGBoost model and produce the optimal weights for each candidate forecasting method, which are used to forecast the Tourism data. Since the Tourism dataset has smaller size compared to the M4 competition data, we use M4 monthly data as the training data for the Tourism monthly data to obtain the optimal weights from XGBoost. The same strategy is applied to the quarterly and yearly datasets.

We apply the same accuracy metrics as in the Tourism competition (Athanasopoulos et al., 2011) to make the results comparable with the literature, which are the mean absolute percentage error (MAPE) and the mean absolute scaled error (MASE). MASE is calculated as Equation (2), and MAPE is calculated as follows.

$$\text{MAPE} = \frac{1}{h} \sum_{t=1}^h \frac{|Y_t - \hat{Y}_t|}{|Y_t|},$$

Table 3. Benchmarking the MASE performance of our proposed forecasting method based on time series imaging against the top 10 methods in the M4 competition.

	Yearly	Quarterly	Monthly	Weekly	Daily	Hourly	Total
Ranking	M4 competition						
1	2.980	1.118	0.884	2.356	3.446	0.893	1.536
2	3.060	1.111	0.893	2.108	3.344	0.819	1.551
3	3.130	1.125	0.905	2.158	2.642	0.873	1.547
4	3.126	1.135	0.895	2.350	3.258	0.976	1.571
5	3.046	1.122	0.907	2.368	3.194	1.203	1.554
6	3.082	1.118	0.913	2.133	3.229	1.458	1.565
7	3.038	1.198	0.929	2.947	3.479	1.372	1.595
8	3.009	1.198	0.966	2.601	3.254	2.557	1.601
9	3.262	1.163	0.931	2.302	3.284	0.801	1.627
10	3.185	1.164	0.943	2.488	3.232	1.049	1.614
Method	Forecasting with time series imaging						
<b>SIFT</b>	3.135	1.125	0.908	2.266	3.463	0.849	1.579
<b>CNN</b>							
<i>Inception-v1+XGBoost</i>	3.096	1.139	0.947	2.479	3.289	1.015	1.592
<i>ResNet-v1-101+XGBoost</i>	3.106	1.147	0.927	2.579	3.377	0.970	1.591
<i>ResNet-v1-50+XGBoost</i>	3.104	1.143	0.917	2.441	3.363	0.965	1.583
<i>VGG-19+XGBoost</i>	3.098	1.133	0.931	2.355	3.235	0.991	1.581

Table 4. Benchmarking the sMAPE performance of our proposed forecasting method based on time series imaging against the top 10 methods in the M4 competition.

	Yearly	Quarterly	Monthly	Weekly	Daily	Hourly	Total
Ranking	M4 competition						
1	13.176	9.679	12.126	7.817	3.170	9.328	11.374
2	13.528	9.733	12.639	7.625	3.097	11.506	11.720
3	13.943	9.796	12.747	6.919	2.452	9.611	11.845
4	13.712	9.809	12.487	6.814	3.037	9.934	11.695
5	13.673	9.816	12.737	8.627	2.985	15.563	11.836
6	13.669	9.800	12.888	6.726	2.995	13.167	11.897
7	13.679	10.378	12.839	7.818	3.222	13.466	12.020
8	13.366	10.155	13.002	9.148	3.041	17.567	11.986
9	13.910	10.000	12.780	6.728	3.053	8.913	11.924
10	13.821	10.093	13.151	8.989	3.026	9.765	12.114
Method	Forecasting with time series imaging						
<b>SIFT</b>	13.896	9.863	12.596	7.899	3.063	11.772	11.816
<b>CNN</b>							
<i>Inception-v1+XGBoost</i>	13.899	9.962	12.659	8.228	3.047	12.521	11.891
<i>ResNet-v1-101+XGBoost</i>	13.917	9.991	12.714	8.277	3.110	12.480	11.914
<i>ResNet-v1-50+XGBoost</i>	13.918	9.973	12.723	8.086	3.123	12.396	11.914
<i>VGG-19+XGBoost</i>	13.872	9.912	12.652	8.294	3.049	12.598	11.853

Table 5. Benchmarking the OWA performance of our proposed forecasting method based on time series imaging against the top 10 methods in the M4 competition.

	Yearly	Quarterly	Monthly	Weekly	Daily	Hourly	Total
Ranking	M4 competition						
1	0.778	0.847	0.836	0.851	1.046	0.440	0.821
2	0.799	0.847	0.858	0.796	1.019	0.484	0.838
3	0.820	0.855	0.867	0.766	0.806	0.444	0.841
4	0.813	0.859	0.854	0.795	0.996	0.474	0.842
5	0.802	0.855	0.868	0.897	0.977	0.674	0.843
6	0.806	0.853	0.876	0.751	0.984	0.663	0.848
7	0.801	0.908	0.882	0.957	1.060	0.653	0.860
8	0.788	0.898	0.905	0.968	0.996	1.012	0.861
9	0.836	0.878	0.881	0.782	1.002	0.410	0.865
10	0.824	0.883	0.899	0.939	0.990	0.485	0.869
Method	Forecasting with time series imaging						
<b>SIFT</b>	0.820	0.858	0.863	0.839	1.009	0.498	0.848
<b>CNN</b>							
<i>Inception-v1+XGBoost</i>	0.814	0.867	0.885	0.895	1.002	0.552	0.854
<i>ResNet-v1-101+XGBoost</i>	0.816	0.872	0.877	0.916	1.025	0.542	0.855
<i>ResNet-v1-50+XGBoost</i>	0.816	0.869	0.873	0.881	1.025	0.538	0.853
<i>VGG-19+XGBoost</i>	0.814	0.863	0.876	0.877	0.994	0.549	0.850

Table 6. Model-averaging results compared with the top methods in the Tourism competition in terms of the MAPE and MASE values.

Forecasting method	MAPE				MASE			
	Yearly	Quarterly	Monthly	Total	Yearly	Quarterly	Monthly	Total
ARIMA	30.639	16.172	21.746	23.444	3.197	1.595	1.495	2.200
ETS	25.065	15.316	20.965	20.745	3.000	1.592	1.526	2.130
THETA	23.409	15.927	22.390	20.688	2.730	1.661	1.649	2.080
SNAIVE	23.610	16.459	22.562	20.988	3.007	1.699	1.631	2.197
DAMPED	27.975	35.830	47.192	35.898	3.061	3.221	3.404	3.209
Forecasting with time series imaging								
<b>SIFT</b>	24.164	<b>15.236</b>	<b>19.984</b>	<b>20.089</b>	2.760	<b>1.570</b>	<b>1.444</b>	<b>2.005</b>
<b>CNN</b>								
<i>Inception-v1+XGBoost</i>	24.633	15.333	<b>20.261</b>	<b>20.383</b>	2.834	<b>1.560</b>	<b>1.467</b>	<b>2.037</b>
<i>ResNet-v1-101+XGBoost</i>	24.288	<b>15.047</b>	<b>20.221</b>	<b>20.142</b>	2.779	<b>1.555</b>	<b>1.468</b>	<b>2.014</b>
<i>ResNet-v1-50+XGBoost</i>	24.347	<b>15.101</b>	<b>19.981</b>	<b>20.117</b>	2.750	<b>1.563</b>	<b>1.454</b>	<b>2.002</b>
<i>VGG-19+XGBoost</i>	23.616	15.599	<b>20.055</b>	<b>20.010</b>	<b>2.689</b>	1.638	<b>1.476</b>	<b>2.008</b>

where  $Y_t$  is the real value of the time series at point  $t$ ,  $\hat{Y}_t$  is the point forecast, and  $h$  is the forecasting horizon.

The top methods in the competition that include ARIMA, ETS, THETA, SNAIVE, and DAMPED are discussed in Athanasopoulos et al. (2011). The first four methods are described in Table 1. DAMPED is a variation of Holt-Winters method that “dampens” the trend to a flat line sometime in the future, and is implemented using `forecast::holt(..., damped=TRUE)` in R. We reproduce these top methods and use them as our benchmarks.

Following the framework in Fig. 6, we obtain the forecasts of the Tourism time series based on time series imaging. Our model averaging results outperforms the top methods from Tourism competition (Athanasopoulos et al., 2011) with high distinctions. Table 6 reports the MASE and MAPE values for our model-averaging method and the top methods from Tourism competition. The numbers in bold indicate that our method is better than the benchmark. Especially, our method performs exceptionally well on monthly and quarterly data. For the yearly dataset, our method is slightly worse, which may be due to the inadequacy of historical data. The optimal parameters of XGBoost on the Tourism competition dataset can be found in Table 8 of Appendix B.

## 5. Discussions

Feature-based time series forecasting has been proved highly promising, primarily through the extraction and selection of an appropriate set of features. Nonetheless, traditional time series feature extraction requires manual design of feature metrics, which is typically complicated to time series forecasting practitioners. Known features used in time series forecasting literature are global characteristic of a time series, which may ignore important local patterns. Evidence from the literature further indicates that feature-based forecast combination might not perform as well as simple averaging when the feature extraction and selection are not properly conducted.

We propose an automated time series imaging feature extraction approach with computer vision algorithms, and our experiment results show that our approach works well for forecast combination. An innovative point of our approach over other feature-based time series forecasting methods is that time series features are extracted automatically from time series imaging, which are obtained using recurrence plots. In principle, any image feature extraction algorithm is applicable to our proposed framework. We employ two widely used algorithms to extract features from time series images, namely the spatial bag-of-features (SBoF) model and the deep convolutional neural networks (CNN).

The SBoF model, combining the scale-invariant feature transform (SIFT) algorithm, the locality constrained linear coding (LLC) method, and spatial pyramid matching (SPM) and max pooling, can capture both global and local characteristics of images. The traditional SBoF model is a fast industry level model in computer vision applications. One may notice that the features extracted based on the traditional SIFT model performs better than the deep CNN model in some scenarios with our testing data. But it is worth to mention that SIFT method is not a fully automated image feature extraction processing because it requires a careful specification of four steps, namely (1) detecting extreme values in the scale spaces, (2) finding the key points, (3) assigning feature directions, and (4) describing key points. Moreover, SIFT algorithm is patent protected (Lowe, 2004), which means other open source program could not incorporate it without the patent owner’s permission. Having an alternative approach with highly comparable performance but without patent restrictions is important to time series forecasters.

The alternative feature extraction algorithm based on deep CNN is an automated process once the source task is confirmed. We use transfer learning to borrow the information of well pre-trained neural network models for imaging classification, which can avoid the complication of settings the network structure and tuning the hyper-parameters. Unlike traditional CNN tasks that require the fine-tuning and massive computation, we transfer the convolutional layers and

fully-connected layers from the ImageNet competition results to our task. Hence only one new adaption layer needs to train, which significantly saves the computational power.

Although the aims of source task in ImageNet and the target task of time series forecasting are naturally different, the image features generated from time series share similar shapes and angles with the image of real objects. This explains why we could transfer a different task to time series forecasting. In practice, the forecasting practitioners may train a customized CNN model to further improve the forecasting performance if a rich collection of time series are available.

Another significant merit of using deep CNN and transfer learning for time series feature extraction is that, the pre-trained neural network models (e.g., on ImageNet) are continuously updated and improved in the image processing literature. Thus, we believe that this line of automated time series feature extraction approaches has great potential in the future.

In this paper, we use the features extracted from recurrence plots to reveal the characteristics of the corresponding time series. The recurrence plot for a given time series displays its dynamics based on the distance correlations within the time series. However, other features such as cross-correlation coefficients can also be used to generate cross-correlation recurrence plots. Thus, multi-channel images, with more comprehensive information, can be obtained for each time series, which can potentially improve the feature extraction and feature-based forecast combination performances. Therefore, time series forecasting based on multi-channel imaging can be one potential extension of our current work.

The forecasting framework based on time series image features is in line with the work in (Montero-Manso et al., 2020), where they use 42 manual time series features and nine forecasting methods to optimize the weights for forecast combination. Montero-Manso et al. (2020) won the second place in the M4 competition (Makridakis et al., 2020). To be consistent and comparable, in our study, we employ the same set of forecasting methods in the M4 dataset. However, we want to mention that the choice of candidate forecasting methods for forecast combination also requires expert knowledge and practical experience. The performance of forecast combinations depends on the accuracy of individual forecasting methods and the diversity among them since the merits of forecast combination stem from the independent information across multiple forecasts (Thomson et al., 2019). How to automatically select an appropriate set of candidate methods for combination is another interesting direction for future research.

In our experiments, all the time series are independent data. Therefore we treat the time series features as independent images and apply them to the CNN framework which is also used for classifying objects in ImageNet. A further extension of our work is to extend time series



forecasting with imaging to (1) forecasting with time varying image features, and (2) hierarchical time series or multivariate time series with recurrent dependence. In both scenes, hierarchical image classification framework mixtures with CNN and RNN could be further explored.

We make our code publicly available at <https://github.com/lixixibj/forecasting-with-time-series-imaging>. Making it open-source can enrich the toolboxes of forecasting support systems by providing a competitive alternative to the existing feature-based time series forecasting methods.

## 6. Concluding remarks

In this paper, we propose to use image features for forecast model combination. First, time series are encoded into images. Computer vision algorithms are then applied to extract features from the images, which are used for forecast model averaging. The proposed method enables automated feature extraction, making it more flexible than using manually selected time series features. Besides, our image features can depict local features of time series as well as global features. Our paper is the first attempt that applies imaging to time series forecasting to the best of our knowledge.

We examined the performance of our approach on two widely-used time series competition datasets (M4 and Tourism), and compared it with the top methods in the two competitions. Our experiments show that the proposed method can produce highly comparable forecast accuracies with the top-ranked benchmarks in the competitions. Moreover, forecasting based on time series imaging offers an automatic tool for time series feature extraction, in the sense that it does not rely on many manual inputs for feature selection, which is crucial for forecast practitioners.

## Acknowledgments

We are thankful to Dr. Slawek Smyl from Uber and Professor Christoph Bergmeir from Monash University for their insightful suggestions on a previous version of this paper presented at the 39th International Symposium on Forecasting.

Yanfei Kang is supported by the National Natural Science Foundation of China (No. 11701022) and the National Key Research and Development Program (No. 2019YFB1404600). Feng Li is supported by the National Natural Science Foundation of China (No. 11501587) and the Beijing Universities Advanced Disciplines Initiative (No. GJJ2019163).

## References

- Abdollahi, M., Khaleghi, T. and Yang, K. (2020), ‘An integrated feature learning approach using deep learning for travel time prediction’, *Expert Systems with Applications* **139**, 112864.
- Ahmad, Z., Jindal, R., Ekbal, A. and Bhattacharyya, P. (2020), ‘Borrow from rich cousin: transfer learning for emotion detection using cross lingual embedding’, *Expert Systems with Applications* **139**, 112851.
- Arinze, B. (1994), ‘Selecting appropriate forecasting models using rule induction’, *Omega-international Journal of Management Science* **22**(6), 647–658.
- Armstrong, J. S. (2001), Combining forecasts, *in* ‘Principles of forecasting’, Springer, pp. 417–439.
- Assimakopoulos, V. and Nikolopoulos, K. (2000), ‘The theta model: a decomposition approach to forecasting’, *International Journal of Forecasting* **16**(4), 521–530.
- Athanasopoulos, G., Hyndman, R. J., Kourentzes, N. and Petropoulos, F. (2017), ‘Forecasting with temporal hierarchies’, *European Journal of Operational Research* **262**(1), 60–74.
- Athanasopoulos, G., Hyndman, R. J., Song, H. and Wu, D. C. (2011), ‘The tourism forecasting competition’, *International Journal of Forecasting* **27**(3), 822–844.
- Bandara, K., Bergmeir, C. and Smyl, S. (2020), ‘Forecasting across time series databases using recurrent neural networks on groups of similar series: a clustering approach’, *Expert Systems With Applications* **140**, 112896.
- Baydogan, M. G., Runger, G. and Tuv, E. (2013), ‘A bag-of-features framework to classify time series’, *IEEE transactions on pattern analysis and machine intelligence* **35**(11), 2796–2802.
- Chen, T. and Guestrin, C. (2016), Xgboost:a scalable tree boosting system, *in* ‘ACM SIGKDD International Conference on Knowledge Discovery and Data Mining’, pp. 785–794.
- Christ, M., Braun, N., Neuffer, J. and Kempa-Liehr, A. W. (2018), ‘Time Series Feature Extraction on basis of Scalable Hypothesis tests (tsfresh a Python package)’, *Neurocomputing* **307**, 72 – 77.
- Cleveland, R. B., Cleveland, W. S., McRae, J. E. and Terpenning, I. (1990), ‘STL: A seasonal-trend decomposition procedure based on loess’, *Journal of Official Statistics* **6**(1), 3–73.
- Collopy, F. and Armstrong, J. S. (1992), ‘Rule-based forecasting: development and validation of an expert systems approach to combining time series extrapolations’, *Management Science* **38**(10), 1394–1414.
- Corizzo, R., Ceci, M., Zdravevski, E. and Japkowicz, N. (2020), ‘Scalable auto-encoders for gravitational waves detection from time series data’, *Expert Systems with Applications* p. 113378.
- De Livera, A. M., Hyndman, R. J. and Snyder, R. D. (2011), ‘Forecasting time series with

- complex seasonal patterns using exponential smoothing’, *Journal of the American statistical association* **106**(496), 1513–1527.
- Deng, J., Dong, W., Socher, R., Li, L. J., Li, K. and Li, F. F. (2009), Imagenet: A large-scale hierarchical image database, *in* ‘IEEE Conference on Computer Vision and Pattern Recognition’.
- Donahue, J., Jia, Y., Vinyals, O., Hoffman, J., Ning, Z., Tzeng, E., Darrell, T., Donahue, J., Jia, Y. and Vinyals, O. (2014), Decaf: A deep convolutional activation feature for generic visual recognition, *in* ‘International Conference on International Conference on Machine Learning’.
- Doornik, J. A., Castle, J. L. and Hendry, D. F. (2020), ‘Card forecasts for m4’, *International Journal of Forecasting* **36**(1), 129–134.
- Eckmann, J.-P., Kamphorst, S. O. and Ruelle, D. (1987), ‘Recurrence plots of dynamical systems’, *EPL (Europhysics Letters)* **4**(9), 973.
- Fiorucci, J. A. and Louzada, F. (2020), ‘Groec: combination method via generalized rolling origin evaluation’, *International Journal of Forecasting* **36**(1), 105–109.
- Fulcher, B. D. (2018), Feature-based time-series analysis, *in* ‘Feature engineering for machine learning and data analytics’, CRC Press, pp. 87–116.
- Fulcher, B. D., Little, M. A. and Jones, N. S. (2013), ‘Highly comparative time-series analysis: the empirical structure of time series and their methods’, *Journal of the Royal Society Interface* **10**(83), 20130048.
- Fulcher, B. and Jones, N. (2014), ‘Highly comparative feature-based time-series classification’, *IEEE Transactions on Knowledge and Data Engineering* **26**(12), 3026–3037.
- Ge, W. and Yu, Y. (2017), Borrowing treasures from the wealthy: Deep transfer learning through selective joint fine-tuning, *in* ‘Computer Vision and Pattern Recognition’.
- Han, D., Liu, Q. and Fan, W. (2018), ‘A new image classification method using cnn transfer learning and web data augmentation’, *Expert Systems With Applications* **95**, 43–56.
- Hatami, N., Gavet, Y. and Debayle, J. (2017), ‘Bag of recurrence patterns representation for time-series classification’, *Pattern Analysis and Applications* pp. 1–11.
- He, K., Zhang, X., Ren, S. and Sun, J. (2016), Deep residual learning for image recognition, *in* ‘Proceedings of the IEEE conference on computer vision and pattern recognition’, pp. 770–778.
- Hyndman, R., Athanasopoulos, G., Bergmeir, C., Caceres, G., Chhay, L., O’Hara-Wild, M., Petropoulos, F., Razbash, S., Wang, E. and Yasmeeen, F. (2019), *forecast: Forecasting functions for time series and linear models*. R package version 8.5.  
**URL:** <http://pkg.robjhyndman.com/forecast>

- Hyndman, R. J. and Khandakar, Y. (2008), ‘Automatic time series forecasting: the forecast package for R’, *Journal of Statistical Software* **26**(3), 1–22.
- Hyndman, R. J., Koehler, A. B., Snyder, R. D. and Grose, S. (2002), ‘A state space framework for automatic forecasting using exponential smoothing methods’, *International Journal of Forecasting* **18**(3), 439–454.
- Hyndman, R. J., Wang, E. and Laptev, N. (2015), Large-scale unusual time series detection, in ‘Proceedings of the IEEE International Conference on Data Mining’, Atlantic City, NJ, USA. 14–17 November 2015.
- Kang, Y., Hyndman, R. J. and Li, F. (2020), ‘GRATIS: GeneRAting Time Series with diverse and controllable characteristics’, *Statistical Analysis and Data Mining* (in press).  
**URL:** <https://doi.org/10.1002/sam.11461>
- Kang, Y., Hyndman, R. J. and Smith-Miles, K. (2017), ‘Visualising forecasting algorithm performance using time series instance spaces’, *International Journal of Forecasting* **33**(2), 345–358.
- Krizhevsky, A., Sutskever, I. and E. Hinton, G. (2012), ‘Imagenet classification with deep convolutional neural networks’, *Neural Information Processing Systems* **25**.
- Laptev, N., Yosinski, J., Li, L. E. and Smyl, S. (2017), Time-series extreme event forecasting with neural networks at uber, in ‘International Conference on Machine Learning’, Vol. 34, pp. 1–5.
- Lazebnik, S., Schmid, C. and Ponce, J. (2006), Beyond bags of features: Spatial pyramid matching for recognizing natural scene categories, in ‘2006 IEEE Computer Society Conference on Computer Vision and Pattern Recognition (CVPR’06)’, Vol. 2, IEEE, pp. 2169–2178.
- Lowe, D. G. (1999), Object recognition from local scale-invariant features, in ‘Computer vision, 1999. The proceedings of the seventh IEEE international conference on’, Vol. 2, IEEE, pp. 1150–1157.
- Lowe, D. G. (2004), ‘Method and apparatus for identifying scale invariant features in an image and use of same for locating an object in an image’. US Patent 6,711,293.
- Maaten, L. v. d. (2014), ‘Accelerating t-SNE using tree-based algorithms’, *The Journal of Machine Learning Research* **15**(1), 3221–3245.
- Makridakis, S. and Hibon, M. (2000), ‘The M3-Competition: results, conclusions and implications’, *International Journal of Forecasting* **16**(4), 451–476.
- Makridakis, S., Spiliotis, E. and Assimakopoulos, V. (2020), ‘The M4 competition: 100,000 time series and 61 forecasting methods’, *International Journal of Forecasting* **36**(1), 54–74.
- Meade, N. (2000), ‘Evidence for the selection of forecasting methods’, *Journal of Forecasting* **19**(6), 515–535.

- Montero-Manso, P., Athanasopoulos, G., Hyndman, R. J. and Talagala, T. S. (2020), ‘FFORMA: Feature-based forecast model averaging’, *International Journal of Forecasting* **36**(1), 86 – 92.
- Nanopoulos, A., Alcock, R. and Manolopoulos, Y. (2001), ‘Feature-based classification of time-series data’, *International Journal of Computer Research* **10**(3).
- Pan, S. J. and Qiang, Y. (2010), ‘A survey on transfer learning’, *IEEE Transactions on Knowledge and Data Engineering* **22**(10), 1345–1359.
- Pawlikowski, M. and Chorowska, A. (2020), ‘Weighted ensemble of statistical models’, *International Journal of Forecasting* **36**(1), 93–97.
- Petropoulos, F., Makridakis, S., Assimakopoulos, V. and Nikolopoulos, K. (2014), ‘Horses for courses’ in demand forecasting’, *European Journal of Operational Research* **237**(1), 152–163.
- Petropoulos, F. and Svetunkov, I. (2020), ‘A simple combination of univariate models’, *International journal of forecasting* **36**(1), 110–115.
- Razavian, A. S., Azizpour, H., Sullivan, J. and Carlsson, S. (2014), ‘Cnn features off-the-shelf: An astounding baseline for recognition’.
- Shah, C. (1997), ‘Model selection in univariate time series forecasting using discriminant analysis’, *International Journal of Forecasting* **13**(4), 489–500.
- Shaub, D. (2020), ‘Fast and accurate yearly time series forecasting with forecast combinations’, *International Journal of Forecasting* **36**(1), 116–120.
- Simonyan, K. and Zisserman, A. (2014), ‘Very deep convolutional networks for large-scale image recognition’, *Computer Science* .
- Smyl, S. (2020), ‘A hybrid method of exponential smoothing and recurrent neural networks for time series forecasting’, *International Journal of Forecasting* **36**(1), 75–85.
- Svetunkov, I. and Kourentzes, N. (2018), ‘Complex exponential smoothing for seasonal time series’.
- Szegedy, C., Liu, W., Jia, Y., Sermanet, P., Reed, S., Anguelov, D., Erhan, D., Vanhoucke, V. and Rabinovich, A. (2015), Going deeper with convolutions, in ‘Proceedings of the IEEE conference on computer vision and pattern recognition’, pp. 1–9.
- Talagala, P. D., Hyndman, R. J., Smith-Miles, K., Kandanaarachchi, S. and Muñoz, M. A. (2019), ‘Anomaly detection in streaming nonstationary temporal data’, *Journal of Computational and Graphical Statistics* (In press), 1–28.
- Talagala, T., Li, F. and Kang, Y. (2019), ‘FFORMPP: Feature-based forecast model performance prediction’, *arXiv* **1908.11500**.
- URL:** <https://arxiv.org/abs/1908.11500>

- Talagala, T. S., Hyndman, R. J. and Athanasopoulos, G. (2018), Meta-learning how to forecast time series, Working paper 6/18, Monash University, Department of Econometrics and Business Statistics.
- Thiel, M., Romano, M. C. and Kurths, J. (2004), ‘How much information is contained in a recurrence plot?’, *Physics Letters A* **330**(5), 343–349.
- Thomson, M. E., Pollock, A. C., Onkal, D. and Gonul, M. S. (2019), ‘Combining forecasts: Performance and coherence’, *International Journal of Forecasting* **35**(2), 474–484.
- Vincent, P., Larochelle, H., Bengio, Y. and Manzagol, P.-A. (2008), Extracting and composing robust features with denoising autoencoders, in ‘Proceedings of the 25th international conference on Machine learning’, pp. 1096–1103.
- Wang, J., Liu, P., She, M. F., Nahavandi, S. and Kouzani, A. (2013), ‘Bag-of-words representation for biomedical time series classification’, *Biomedical Signal Processing and Control* **8**(6), 634–644.
- Wang, J., Yang, J., Yu, K., Lv, F., Huang, T. and Gong, Y. (2010), Locality-constrained linear coding for image classification, in ‘Computer Vision and Pattern Recognition (CVPR), 2010 IEEE Conference on’, IEEE, pp. 3360–3367.
- Wang, X., Smith, K. A. and Hyndman, R. J. (2006), ‘Characteristic-based clustering for time series data’, *Data Mining and Knowledge Discovery* **13**(3), 335–364.
- Wang, Z. and Oates, T. (2015), Imaging time-series to improve classification and imputation, in ‘Proceedings of the 24th International Conference on Artificial Intelligence’, AAAI Press, pp. 3939–3945.

## Appendices

### A. Experimental setup in the SoBF model and CNN model

In the traditional image processing method with SIFT, we need to obtain the basic descriptors before the linear coding. We choose  $k = 200$  as the number of clusters, 200 centroid coordinates are used as the coordinates of basic descriptors. We select 5 close descriptors from 200 basic descriptors for each descriptor with the K-nearest neighbors (KNN) algorithm and the adjustment factor  $\lambda = e^{-4}$  in LLC. We set 1, 2, and 4 as the SPM parameters. In the end, we split the image into  $1 \times 1$ ,  $2 \times 2$  and  $4 \times 4$  subimages, respectively. To eliminate range differences of time series, we further adopt the minimax transformation for time series before applying the recurrence plot. The parameter of  $\epsilon$  for recurrence plot generation is 0.5.

Table 7. Optimal parameters of XGBoost on M4 competition dataset.

Method	max_depth	learning_rate	sample_proportion	feature_proportion
<b>SIFT</b>	14.000	0.575	0.916	0.767
<b>CNN</b>				
<i>Inception-v1+XGBoost</i>	15.000	0.600	0.920	0.810
<i>ResNet-v1-101+XGBoost</i>	20.000	0.660	0.892	0.871
<i>ResNet-v1-50+XGBoost</i>	18.000	0.640	0.960	0.850
<i>VGG-19+XGBoost</i>	12.000	0.530	0.940	0.830

The parameters for the pre-trained CNN models are set as follows.

- Dimension of the output of the pre-trained *Inception-v1* model: 1024.
- Dimension of the output of the pre-trained *ResNet-v1-101* model: 2048.
- Dimension of the output of the pre-trained *ResNet-v1-50* model: 2048.
- Dimension of the output of the pre-trained *VGG* model: 1000.

## B. Experimental setup for XGBoost

To set optimal parameters for XGBoost, we perform a search in subspaces of the hyper-parameter spaces, by measuring the OWA via 10-fold cross-validation of the training data. We describe the hyper-parameters and the searching ranges of the cross-validation procedure as follows.

- **max\_depth**: The maximum depth of a tree ranges from 6 to 25.
- **learning\_rate**: The learning rate and the scale of contribution of each tree ranges from 0.01 to 1.
- **sample\_proportion**: The proportion of the training set used to calculate the trees in each iteration ranges from 0.7 to 1.
- **feature\_proportion**: The proportion of features used to calculate the trees in each iteration ranges from 0.7 to 1.

Table 7 reports the optimal parameters of XGBoost on the M4 competition dataset. In the experiment, we train the XGBoost with all data of different periods and as a result get one set of optimal parameters.

Table 8 shows the optimal parameters of XGBoost for yearly, quarterly and monthly, respectively on the Tourism competition dataset. Due to the small size of Tourism dataset, we use



Table 8. Optimal parameters of XGBoost on Tourism competition dataset.

Method	max_depth	learning_rate	sample_proportion	feature_proportion
Yearly				
<b>SIFT</b>	25.000	1.000	0.747	1.000
<b>CNN</b>				
<i>Inception-v1+XGBoost</i>	12.000	0.907	0.700	1.000
<i>ResNet-v1-101+XGBoost</i>	6.000	1.000	0.967	0.866
<i>ResNet-v1-50+XGBoost</i>	7.000	0.872	0.747	0.976
<i>VGG-19+XGBoost</i>	8.000	0.877	0.960	0.710
Quarterly				
<b>SIFT</b>	12.000	0.880	0.851	0.861
<b>CNN</b>				
<i>Inception-v1+XGBoost</i>	17.000	0.856	1.000	0.700
<i>ResNet-v1-101+XGBoost</i>	8.000	0.985	0.985	0.947
<i>ResNet-v1-50+XGBoost</i>	14.000	0.581	0.921	0.781
<i>VGG-19+XGBoost</i>	11.000	0.872	0.858	0.764
Monthly				
<b>SIFT</b>	14.000	0.575	0.916	0.767
<b>CNN</b>				
<i>Inception-v1+XGBoost</i>	25.000	1.000	0.861	0.700
<i>ResNet-v1-101+XGBoost</i>	25.000	1.000	1.000	1.000
<i>ResNet-v1-50+XGBoost</i>	14.000	1.000	1.000	0.705
<i>VGG-19+XGBoost</i>	17.000	0.842	0.935	0.913

M4 data with the corresponding periods as the training data. Hence, we obtain three groups of optimal parameters for yearly, quarterly and monthly data, respectively.